Multicriticality, metastability, and the roton feature in Bose-Einstein condensates with three-dimensional spin-orbit coupling

Renyuan Liao,[1] Oleksandr Fialko,[2] Joachim Brand,[3] and Ulrich Zülicke[4]

[1]*Fujian Provincial Key Laboratory of Quantum Manipulation and New Energy Materials, College of Physics and Energy, Fujian Normal University, Fuzhou 350117, China*

[2]*Institute of Natural and Mathematical Sciences and Centre for Theoretical Chemistry and Physics, Massey University Auckland, Private Bag 102904, North Shore, Auckland 0745, New Zealand*

[3]*New Zealand Institute for Advanced Study, Dodd-Walls Centre for Photonics and Quantum Technology, and Centre for Theoretical Chemistry and Physics, Massey University Auckland, Private Bag 102904, North Shore, Auckland 0745, New Zealand*

[4]*School of Chemical and Physical Sciences and Dodd-Walls Centre for Photonics and Quantum Technology, Victoria University of Wellington, PO Box 600, Wellington 6140, New Zealand*

(Received 25 April 2015; published 30 October 2015)

We theoretically study homogeneously trapped atomic Bose-Einstein condensates where all three-momentum components couple to a pseudo-spin-$\frac{1}{2}$ degree of freedom. Tuning the anisotropies of spin-orbit coupling and the spin-dependent interactions is shown to provide access to a rich phase diagram with a tetracritical point, first-order phase transitions, and multiple metastable phases of stripe and plane-wave character. The elementary excitation spectrum of the axial plane-wave phase features an anisotropic roton feature and can be used to probe the phase diagram. In addition to providing a versatile laboratory for studying fundamental concepts in statistical physics, the emergence of metastable phases creates new opportunities for observing false-vacuum decay and bubble nucleation in ultracold-atom experiments.

DOI: 10.1103/PhysRevA.92.043633 PACS number(s): 67.85.Fg, 03.75.Mn, 05.30.Jp, 67.85.Jk

Introduction. The possibility to create artificial gauge fields in neutral ultracold-atom systems [1,2] has drastically expanded the array of possibilities for highly controlled experimental simulation of quantum many-particle systems [2,3]. In particular, it has become possible to explore effects associated with spin-orbit coupling (SOC) [4] that give rise to intriguing phenomena such as the quantum spin Hall effect [5–8], new materials classes such as topological insulators and superconductors [7–10], and exotic quasiparticle excitations such as Majorana fermions [11–13]. In bosonic-atom systems, the presence of SOC was found to generate novel ground states that have no known analogs in conventional solid-state materials [14–16]. Intense theoretical attention has focused on the many-body physics of spin-orbit-coupled Bose-atom systems in free space [17–23] and in harmonic traps [24–30]. To date, several types of SOC have been realized in the laboratory, including one-dimensional (1D) SOC involving a single Cartesian component of the atoms' momentum [31–34], and two-dimensional (2D) SOC [35]. However, several proposals exist for creating a three-dimensional (3D) Rashba-type SOC [36–38]. The three-dimensional analog of Rashba SOC is interesting because it is expected to stabilize a long-sought Skyrmion mode in the ground state of trapped Bose-Einstein condensates (BECs) [27,30]. The intriguing possibility to simulate the so-called Weyl SOC (which is a spherically symmetric 3D Rashba SOC analog) has also been suggested [36].

Despite the rapid pace of theoretical and experimental studies in the field of spin-orbit-coupled atom gases, the physical properties of an extended interacting Bose system in the presence of 3D SOC has received very little attention with only part of the ground-state phase diagram known [21]. This clearly presents a significant gap in our basic understanding, because the extended system's behavior constitutes an important benchmark for identifying effects associated solely with trapping potentials. Furthermore, real experimental systems can be designed with a flat-bottom potential to approximate the extended system and give access to the intriguing physics demonstrated by our present study [39]. In particular, we show that 3D SOC in an interacting Bose gas leads to a highly nontrivial phase diagram featuring a tetracritical point [40], first-order phase transitions, and emergent metastable phases. Thus this system provides opportunities to study ramifications of multicriticality [41] and metastability, including false-vacuum decay and bubble nucleation [42–45], in ultracold-atom experiments. We have also studied the spectrum of elementary excitations and find it to be useful for probing the multitude of phases and phase transitions.

The model. We consider a 3D homogeneous interacting two-component Bose gas subject to cylindrically symmetric spin-orbit coupling, described by the Hamiltonian $H = H_0 + H_{\rm I}$, with

$$H_0 = \int d^3r\, \Psi^\dagger(\mathbf{r}) \left[\frac{\hat{\mathbf{p}}^2}{2m} + \lambda(\hat{\sigma}_\perp \cdot \hat{\mathbf{p}}_\perp + \gamma \hat{\sigma}_z \hat{p}_z) \right] \Psi(\mathbf{r}), \quad \text{(1a)}$$

$$H_{\rm I} = \int d^3r \left[g \sum_\sigma n_\sigma^2(\mathbf{r}) + 2 g_{\uparrow\downarrow} n_\uparrow(\mathbf{r}) n_\downarrow(\mathbf{r}) \right]. \quad \text{(1b)}$$

Here $\Psi(\mathbf{r}) = (\psi_\uparrow, \psi_\downarrow)^T$ is a two-component spinor field, $n_\sigma = \psi_\sigma^\dagger \psi_\sigma$ is the density for component $\sigma \in \{\uparrow, \downarrow\}$, m is the atomic mass, $\hat{\sigma}_j$ (with $j = x, y, z$) denote the Pauli matrices and $\hat{p}_j = -i\hbar \hat{\nabla}_j$ are the Cartesian components of the single-atom momentum operator $\hat{\mathbf{p}}$.

The parameter λ measures the SOC strength involving the momentum $\hat{\mathbf{p}}_\perp$ in the xy plane, and the dimensionless number γ describes the anisotropy of SOC for the momentum

component parallel to the z direction. Note that the limit $\gamma = 0$ is the unitary equivalent of the conventional Rashba SOC [1], $\gamma = 1$ realizes the so-called Weyl SOC [36], and a situation corresponding to the experimentally created 1D SOC [31–34] is obtained when $\gamma \to \infty$ (with $\lambda\gamma$ finite). Fundamentally, the parameter γ could be tuned by a sequence of pulsed inhomogeneous magnetic fields [36]. Also, the strength g ($g_{\uparrow\downarrow}$) of interactions between same-spin (opposite-spin) components can be varied by using an appropriate Feshbach resonance [46]. In the special case when $\gamma = 1$ and $g = g_{\uparrow\downarrow}$, the Hamiltonian H is symmetric with respect to simultaneous rotations of the internal pseudo-spin-$\frac{1}{2}$ degree of freedom and the particle momentum. Throughout the rest of the paper, we use units such that $\hbar = k_B = 2m = 1$.

Diagonalization of H_0 yields the two-branch single-particle energy spectrum $E_\pm(\mathbf{p}) = (p \pm \lambda\tau_\mathbf{p}/2)^2 - \lambda^2\tau_\mathbf{p}^2/4$ as a function of 3D momentum $\mathbf{p}$. Using spherical coordinates, $\mathbf{p} \equiv (p\sin\theta_\mathbf{p}\cos\varphi_\mathbf{p}, p\sin\theta_\mathbf{p}\sin\varphi_\mathbf{p}, p\cos\theta_\mathbf{p})$, we have $\tau_\mathbf{p} = (\gamma^2\cos^2\theta_\mathbf{p} + \sin^2\theta_\mathbf{p})^{1/2}$, and the eigenspinors are given by

$$\Psi_\pm(\mathbf{p}) = \begin{pmatrix} \frac{\pm\sin\theta_\mathbf{p}}{\sqrt{\tau_\mathbf{p}\mp\gamma\cos\theta_\mathbf{p}}}e^{-i\varphi_\mathbf{p}} \\ \sqrt{\tau_\mathbf{p}\mp\gamma\cos\theta_\mathbf{p}} \end{pmatrix} \frac{e^{i\mathbf{p}\cdot\mathbf{r}}}{\sqrt{2\tau_\mathbf{p}}}. \tag{2}$$

The lowest-energy state for a given propagation direction parametrized by $\theta_\mathbf{q}$ and $\varphi_\mathbf{q}$ is from the "$-$" branch and occurs at the momentum $\mathbf{q}$ satisfying $q = \lambda\tau_\mathbf{q}/2$.

The phase diagram. To determine the ground state of the interacting system, as it is routinely done in the literature [15,20], we assume that the system has condensed into a coherent superposition of two plane-wave states with momenta $\pm\mathbf{q}$ having magnitude $q = \lambda\tau_\mathbf{q}/2$ [47]. Thus the condensate wave function has the form $\Phi_0 = C_+\Psi_-(\mathbf{q}) + C_-\Psi_-(-\mathbf{q})$, with coefficients $C_\pm$ that will be determined by a variational procedure. The condition $n_0 = |C_+|^2 + |C_-|^2$, with n_0 being the particle number density, suggests the parametrization $|C_+|^2 = n_0\cos^2(\alpha/2)$ and $|C_-|^2 = n_0\sin^2(\alpha/2)$, with $\alpha \in [0,\pi]$. Introducing the dimensionless nonlinear-coupling parameter $\tilde{g} \equiv (g_{\uparrow\downarrow} - g)n_0/\lambda^2$ and volume of the system $\mathcal{V}$, we find the variational ground-state energy density $E_g \equiv \langle\Phi_0|H|\Phi_0\rangle/\mathcal{V} - gn_0$ given by

$$\frac{E_g}{\lambda^2 n_0} = -\frac{\tau_\mathbf{q}^2}{4} + \frac{\tilde{g}}{2}\left[\sin^2\alpha\left(1 - \frac{3\sin^2\theta_\mathbf{q}}{2\tau_\mathbf{q}^2}\right) + \frac{\sin^2\theta_\mathbf{q}}{\tau_\mathbf{q}^2}\right]. \tag{3}$$

To see that such an energy expression may recover known results, we first consider the familiar case of 2D SOC by setting $\gamma = 0$. Minimization of E_g with respect to $\theta_\mathbf{q}$ and α then yields $\sin^2\theta_\mathbf{q} = 1$ and $\sin^2\alpha = 1$ (0) for $\tilde{g} > 0$ ($\tilde{g} < 0$). The first condition implies that the condensation momentum is pinned in the xy plane, and the latter condition yields the stripe phase for $\tilde{g} > 0$ ($|C_+| = |C_-|$, i.e., condensation in a coherent superposition of the opposite-momentum states) or the plane-wave phase for $\tilde{g} < 0$ (either $|C_+| = 0$ or $|C_-| = 0$, i.e., condensation at only one momentum eigenstate). We thus reproduce the ground-state structure of the conventional two-dimensional-Rashba SOC case [15,21].

Setting $\gamma \neq 0$ unpins the condensation momentum from the xy plane, making it possible to condense into a state whose momentum has a finite z component. In the following, we will term such condensation as "polar," while condensation into a momentum that lies in the xy plane will be called "axial". As each of these cases can support a stripe (SP) or plane-wave (PW) condensate, depending on the interaction strength $\tilde{g}$, we have four distinct possible phases: PW axial, SP axial, PW polar, and SP polar. Examination of the variational ground-state-energy landscape shows that each of the four phases is found to be either a true ground state or a metastable state, depending on the values of $\tilde{g}$ and γ. See Fig. 1 for pertinent examples. The basic features of the ground-state phase diagram for $0 \leqslant \gamma^2 \leqslant 1$ have previously been discussed in Ref. [21]. The emergence of stable and metastable phases as global or local minima of the energy landscape is verified by checking the positivity of the Hessian matrix

$$h_E = \begin{pmatrix} \frac{\partial^2 E_g}{\partial\theta_\mathbf{q}^2} & \frac{\partial E_g}{\partial\theta_\mathbf{q}}\frac{\partial E_g}{\partial\alpha} \\ \frac{\partial E_g}{\partial\theta_\mathbf{q}}\frac{\partial E_g}{\partial\alpha} & \frac{\partial^2 E_g}{\partial\alpha^2} \end{pmatrix}. \tag{4}$$

This criterion, however, is not yet sufficient to prove the (meta) stability of a given phase. We thus also consider the elementary excitation spectrum, where imaginary frequencies indicate any instabilities.

The true ground-state phase diagram spanned by tuning parameters $\tilde{g}$ and γ^2 is shown in Fig. 2. A tetracritical point Q_c connecting the four possible phases emerges when $\tilde{g} = 0$

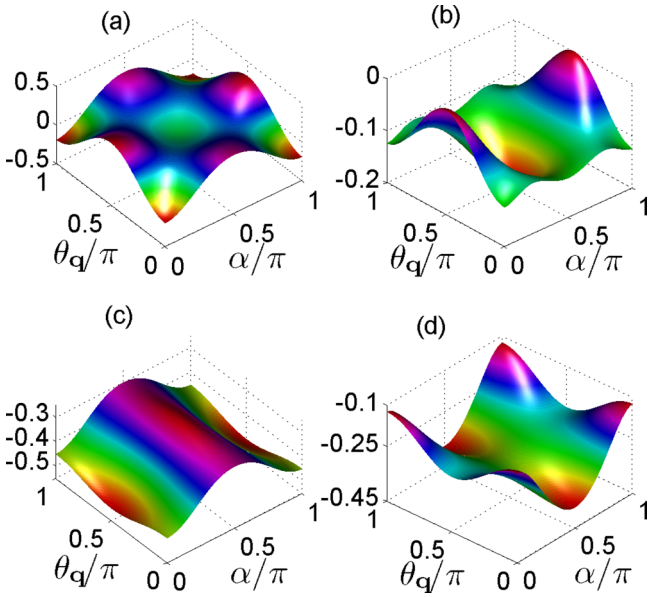

FIG. 1. (Color online) The ground-state energy density E_g in units of $\lambda^2 n_0$ as a function of the variational parameters $\theta_\mathbf{q}$ and α for particular values of the interaction anisotropy $\tilde{g}$ and the SOC strength λ: (a) $\tilde{g} = 1.0$ and $\gamma^2 = 0.8$, PW polar ($\theta_\mathbf{q} = 0 = \alpha$); (b) $\tilde{g} = 0.25$ and $\gamma^2 = 0.5$, SP axial ($\theta_\mathbf{q} = \pi/2 = \alpha$); (c) $\tilde{g} = -0.1$ and $\gamma^2 = 1.8$, SP polar ($\theta_\mathbf{q} = \pi/2, \alpha = 0$); and (d) $\tilde{g} = -0.25$ and $\gamma^2 = 0.5$, PW axial ($\theta_\mathbf{q} = 0, \alpha = \pi/2$). The phases have been assigned according to the $\theta_\mathbf{q}$ and α values of the global minimum, which corresponds to the ground state. Additional local minima signify the existence of metastable phases in panel (a) as SP Axial and in panel (b) as PW Polar, while there are no metastable phases for panels (c) and (d). Existence regimes of ground-state and metastable phases are shown in Figs. 2 and 3, respectively.

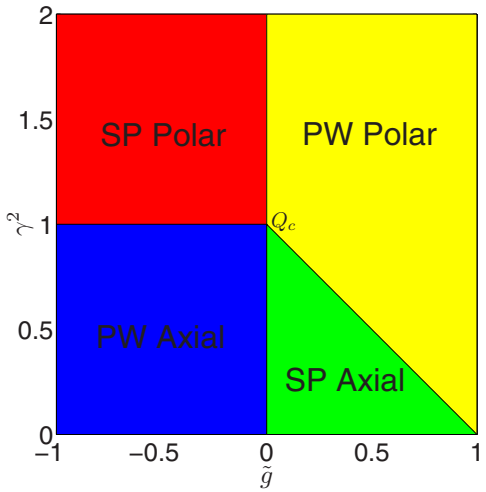

FIG. 2. (Color online) Phase diagram controlled by varying the parameter $\tilde{g}$ that measures anisotropy of spin-dependent interaction strengths and the quantity γ^2 related to anisotropy of spin-orbit coupling. Four possible phases exist—PW polar, SP polar, PW axial, and SP axial—that intersect at the tetracritical point Q_c. For polar (axial) phases, the condensate momentum has a finite (vanishing) z component. In the PW (SP) phases, condensation occurs into a single (a superposition of two) plane-wave state(s).

and $\gamma = 1$. At this high-symmetry point, the system is invariant with respect to simultaneous SU(2) spin rotation and rotation of the momentum of the atoms. The observed behavior at Q_c in our system contrasts with that exhibited in the presence of a tight harmonic trapping potential where Skyrmion textures are stabilized in the ground state [27].

The lowest dynamically stable metastable states are shown in Fig. 3. They gradually disappear as the parameter γ^2 approaches zero, in the sense that local minima in Fig. 1 cease to exist at this point. This means that metastable phases literally emerge in Bose-Einstein condensates with 3D SOC

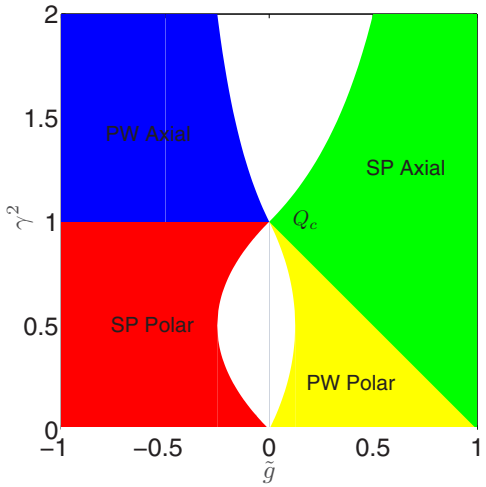

FIG. 3. (Color online) The phase diagram of metastable states controlled by $\tilde{g}$ and γ^2. White regions indicate parameter combinations for which no dynamically stable metastable phases exist, i.e., where the Hessian matrix in Eq. (4) is not positive definite.

only. The presence of metastable phases along with the true ground states creates the opportunity to simulate false-vacuum decay. Proposed by Coleman for modeling phase transitions in the universe [43], decay from a false vacuum into a true one plays a key role in numerous physical contexts. For example, it occurs in a superheated liquid, where the false vacuum is the liquid state, while the true one is gaseous [44]. Thermodynamic fluctuations trigger the continuous appearance of vapor bubbles in the liquid. Eventually, growing bubbles swallow the entire system. More speculative manifestations of the phenomena exist also in modern cosmology [48,49]. Due to the its high tunability, our system provides an easy route toward testing the false-vacuum quantum decay. The system can be prepared initially in one of the metastable phases of Fig. 3. Quantum fluctuations are then expected to trigger quantum decay accompanied with nucleation of bubbles of one of the lower-lying true ground states.

Elementary excitations. The phases and phase transitions in our system can be probed by studying the spectrum of elementary excitations, e.g., by using Bragg spectroscopy [50–53]. Here we consider the elementary excitations around the PW-axial ground state; partly motivated by the fact that, for the case of one-dimensional SOC, interesting roton-like modes were found [20]. Physically, the roton mode signals a system's tendency to undergo a first-order phase transition to a supersolid when the roton gap closes [20,54], and it is usually the consequence of strong correlations in the system due to the interplay of SOC and interactions. Our aim is to show that these features persist also in the case of 3D SOC and that it probes the rich phase diagram obtained above.

The PW axial phase has one condensation momentum lying in the xy plane. Without loss of generality, we choose the condensate momentum to be $\boldsymbol{\kappa} = \frac{\lambda}{2}(-1,0,0)$. Within the framework of imaginary-time functional integration, the partition function of the system reads [55] $\mathcal{Z} = \int \mathcal{D}[\Psi^*,\Psi] \exp(-S[\Psi^*,\Psi])$ with the action $S[\Psi^*,\Psi] = \int_0^\beta d\tau [\int d^3r \sum_\sigma \Psi_\sigma^* \partial_\tau \Psi_\sigma + H - \mu N]$, where $\beta = 1/T$ is the inverse temperature, and μ is the chemical potential introduced to fix the total particle number. The Bose field is split into the mean-field and fluctuating parts, $\Psi_{\mathbf{q}\sigma} = \Phi_{0\sigma}|_{\mathbf{q}=\boldsymbol{\kappa}} + \phi_{\mathbf{q}\sigma}$. We then expand the action of the system up to the quadratic order in fluctuating fields, obtaining an effective action $S_{\text{eff}} \simeq S_0 + S_g$. Here $S_0 = \mathcal{V} \sum_\sigma [(-\frac{\lambda^2}{4} - \mu) n_{0\sigma} + (g + g_{\uparrow\downarrow}) n_{0\sigma}^2]$ is the mean-field contribution, while $S_g = \frac{1}{2} \Phi_{\mathbf{q}}^\dagger \mathcal{G}^{-1} \Phi_{\mathbf{q}}$ is the fluctuating contribution with a vector field $\Phi_{\mathbf{q}} = (\phi_{\tilde{\kappa}+\mathbf{q}\uparrow}, \phi_{\tilde{\kappa}+\mathbf{q}\downarrow}, \phi^*_{\tilde{\kappa}-\mathbf{q}\uparrow}, \phi^*_{\tilde{\kappa}-\mathbf{q}\downarrow})^T$. $\mathcal{G}^{-1}$ is the inverse Green's function of the elementary excitations defined as

$$\mathcal{G}^{-1} = \begin{pmatrix} -iw_n + \epsilon_{\mathbf{q}}^+ & R_{\mathbf{q}} & gn_0 & g_{\uparrow\downarrow} n_0 \\ R_{\mathbf{q}}^* & -iw_n + \epsilon_{\mathbf{q}}^- & g_{\uparrow\downarrow} n_0 & gn_0 \\ gn_0 & g_{\uparrow\downarrow} n_0 & iw_n + \epsilon_{-\mathbf{q}}^+ & R_{-\mathbf{q}}^* \\ g_{\uparrow\downarrow} n_0 & gn_0 & R_{-\mathbf{q}} & iw_n + \epsilon_{-\mathbf{q}}^- \end{pmatrix}, \tag{5}$$

where $\epsilon_{\mathbf{q}}^\pm = q^2 + \frac{\lambda^2}{2} + \lambda(\pm\gamma q_z - q_x) + gn_0$ and $R_{\mathbf{q}} = g_{\uparrow\downarrow} n_0 + \lambda(-\frac{\lambda}{2} + q_x - iq_y)$.

The spectrum of the elementary excitations is determined from the poles of the Green's function. There are two branches

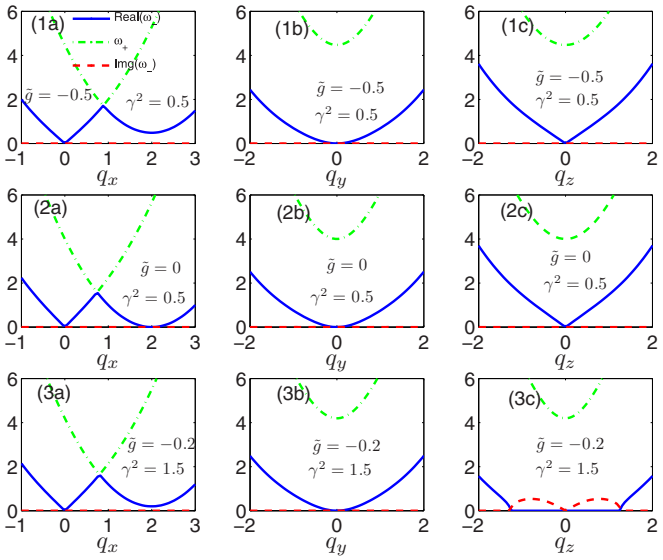

FIG. 4. (Color online) Dispersion of low-lying elementary excitations $\omega_{\pm}$ along q_x (left panels), q_y (center panels), and q_z (right panels). First row: $\tilde{g} = -0.5$ and $\gamma^2 = 0.5$ (PW axial phase is stable), a phonon-maxon-roton feature is seen along the x direction. Second row: $\tilde{g} = 0$ and $\gamma^2 = 0.5$ (boundary between PW axial and SP axial phases), the roton minimum goes soft. Third row: $\tilde{g} = -0.2$ and $\gamma^2 = 1.5$ (metastability of the PW axial phase is broken), imaginary parts appear in q_z dispersion. We have set $gn_0/\lambda^2 = 0.25$ in all panels.

of excitations found as illustrated in Fig. 4. We choose parameters to probe the PW axial ground state and show the results in the first row in Fig. 4. The lower branch of the spectrum exhibits a typical linear Bogoliubov slope at low momenta, followed by a roton and maxon features at higher momenta. This structure of the spectrum persists whenever the momentum $\mathbf{q}$ has components along the axis of the condensation, in this case the x axis. The roton-maxon feature is absent along any direction that is perpendicular to the direction of condensation momentum. There is a conical intersection at around $q_x = 1$, reflecting the time-reversal symmetry of the system. It can be lifted by a Zeeman-like field in the Hamiltonian, in which case the lower branch will become separated from the upper one. Our purpose here is to study how the spectrum changes when we drive the system across the phase diagram.

When the system is driven close to the boundary with the SP axial phase, the roton minimum becomes soft as shown in the second row of Fig. 4. This signals the instability of the system toward the striped order, whose spatial modulation is set by the momentum at which the gap closes. There are no metastable phases at this boundary, as shown in Fig. 3. This phase transition is of second order. On the other hand, nothing dramatic occurs when we move close to the boundary with the SP polar phase. The roton gap does not close, and the spectrum of the PW axial phase does not show any specific feature at the phase boundary. This is due to the presence of metastable phases and also proves the stability of the (metastable) PW axial phase by the absence of imaginary Bogoliubov frequencies. The PW axial phase becomes metastable when we cross the line $\gamma^2 = 1$ at fixed $\tilde{g} < 0$ from below, as shown in Fig. 3. Therefore, this phase transition is first order. We need to drive the system much further to see changes in the excitation spectrum; namely, until the point when metastability breaks down as shown in the third row of Fig. 4. The spectrum of the SP phase is qualitatively different from the PW axial phase and features a double-gapless band structure due to spontaneously broken translations symmetry, as shown in Ref. [54]. Therefore, measuring the excitation spectrum can be used as a probe of the rich phase diagram in the presence of 3D SOC.

It is interesting to note that, at the tetracritical point Q_c, we find also two gapless Goldstone modes, resulting, however, from spontaneous breaking of spin-rotation symmetry and U(1) gauge symmetry [21]. Such modes are expected to remove the four-fold degeneracy at Q_c found at the mean-field level, leading to a unique ground state via the so-called "order from disorder" mechanism [26,56]. Note that the authors of Ref. [21] concluded that BEC is destroyed near the tetracritical point at finite temperature.

Experimental relevance. For a trapped Bose gas in the presence of Weyl SOC and weak interparticle interaction, one expects that the ground state is a Skyrmion, which is a superposition of the few lowest Landau levels [27]. Our predictions should apply for flat-bottom traps as in Ref. [39]. In addition, we may expect the main features of the presented phase diagram be present in harmonic traps with sufficiently strong nonlinearity [30]. To simulate the false vacuum decay, one may first prepare the condensate in a part of the phase diagram where metastable states do not exist. By tuning the control parameters $\tilde{g}$ and γ^2 one can subsequently drive the system into a metastable state. In order to estimate the appropriate parameter regimes, temperatures, and driving speed it will be useful to consider the thermal and quantum depletion of the condensate [21].

Acknowledgments. R.L. acknowledges funding from the NSFC under Grants No. 11274064 and NCET-13-0734. O.F. was supported by the Marsden Fund (contract MAU1205), administered by the Royal Society of New Zealand.

[1] J. Dalibard, F.Gerbier, G. Juzeliūnas, and P. Öhberg, Rev. Mod. Phys. **83**, 1523 (2011).
[2] N. Goldman, G. Juzeliūnas, P. Öhberg, and I. B. Spielman, Rep. Prog. Phys. **77**, 126401 (2014).
[3] I. Bloch, J. Dalibard, and S. Nascimbène, Nat. Phys. **8**, 267 (2012).
[4] V. Galitski and I. B. Spielman, Nature (London) **494**, 49 (2013).
[5] C. L. Kane and E. J. Mele, Phys. Rev. Lett. **95**, 226801 (2005).
[6] B. A. Bernevig and S.-C. Zhang, Phys. Rev. Lett. **96**, 106802 (2006).
[7] B. A. Bernevig, T. L. Hughes, and S. C. Zhang, Science **314**, 1757 (2006).
[8] M. König, S. Wiedmann, C. Brüne, A. Roth, H. Buhmann, L. W. Molenkamp, X. Qi, and S. Zhang, Science **318**, 766 (2007).

[9] M. Z. Hasan and C. L. Kane, Rev. Mod. Phys. **82**, 3045 (2010).
[10] X.-L. Qi and S.-C. Zhang, Rev. Mod. Phys. **83**, 1057 (2011).
[11] J. Alicea, Rep. Prog. Phys. **75**, 076501 (2012).
[12] C. Beenakker, Annu. Rev. Condens. Matter Phys. **4**, 113 (2013).
[13] S. R. Elliott and M. Franz, Rev. Mod. Phys. **87**, 137 (2015).
[14] T. D. Stanescu, B. Anderson, and V. Galitski, Phys. Rev. A **78**, 023616 (2008).
[15] C. Wang, C. Gao, C. M. Jian, and H. Zhai, Phys. Rev. Lett. **105**, 160403 (2010).
[16] T.-L. Ho and S. Zhang, Phys. Rev. Lett. **107**, 150403 (2011).
[17] R. Barnett, S. Powell, T. Grass, M. Lewenstein, and S. Das Sarma, Phys. Rev. A **85**, 023615 (2012).
[18] T. A. Sedrakyan, A. Kamenev, and L. I. Glazman, Phys. Rev. A **86**, 063639 (2012).
[19] T. Ozawa and G. Baym, Phys. Rev. Lett. **109**, 025301 (2012).
[20] Y. Li, L. P. Pitaevskii, and S. Stringari, Phys. Rev. Lett. **108**, 225301 (2012).
[21] X. Cui and Q. Zhou, Phys. Rev. A **87**, 031604(R) (2013).
[22] R. Liao, Z.-G. Huang, X.-M. Lin, and W.-M. Liu, Phys. Rev. A **87**, 043605 (2013); R. Liao, Z.-G. Huang, X.-M. Lin, and O. Fialko, *ibid.* **89**, 063614 (2014).
[23] O. Fialko, J. Brand, and U. Zülicke, New J. Phys **16**, 025006 (2014).
[24] S. Sinha, R. Nath, and L. Santos, Phys. Rev. Lett. **107**, 270401 (2011).
[25] X.-Q. Xu and J. H. Han, Phys. Rev. Lett. **108**, 185301 (2012).
[26] H. Hu, B. Ramachandhran, H. Pu, and X.-J. Liu, Phys. Rev. Lett. **108**, 010402 (2012).
[27] T. Kawakami, T. Mizushima, M. Nitta, and K. Machida, Phys. Rev. Lett. **109**, 015301 (2012).
[28] Z. F. Xu, Y. Kawaguchi, L. You, and M. Ueda, Phys. Rev. A **86**, 033628 (2012).
[29] S.-W. Su, I.-K. Liu, Y.-C. Tsai, W. M. Liu, and S.-C. Gou, Phys. Rev. A **86**, 023601 (2012).
[30] X. Zhou, Y. Li, Z. Cai, and C. Wu, J. Phys. B **46**, 134001 (2013).
[31] Y.-J. Lin, K. Jiménez-Garcia, and I. B. Spielman, Nature (London) **471**, 83 (2011).
[32] J. Y. Zhang, S. C. Ji, Z. Chen, L. Zhang, Z. D. Du, B. Yan, G. S. Pan, B. Zhao, Y. J. Deng, H. Zhai, S. Chen, and J. W. Pan, Phys. Rev. Lett. **109**, 115301 (2012).
[33] P. Wang, Z.-Q. Yu, Z. Fu, J. Miao, L. Huang, S. Chai, H. Zhai, and J. Zhang, Phys. Rev. Lett. **109**, 095301 (2012).
[34] L. W. Cheuk, A. T. Sommer, Z. Hadzibabic, T. Yefsah, W. S. Bakr, and M. W. Zwierlein, Phys. Rev. Lett. **109**, 095302 (2012).
[35] L.-H. Huang, Z.-M. Meng, P.-J. Wang, P. Peng, S.-L. Zhang, L.-C. Chen, D.-h. Li, Q. Zhou, and J. Zhang, arXiv:1506.02861.
[36] B. M. Anderson, G. Juzeliūnas, V. M. Galitski, and I. B. Spielman, Phys. Rev. Lett. **108**, 235301 (2012).
[37] Y. Li, X. Zhou, and C. Wu, Phys. Rev. B **85**, 125122 (2012).
[38] Z.-F. Xu, L. You, and M. Ueda, Phys. Rev. A **87**, 063634 (2013).
[39] A. L. Gaunt, T. F. Schmidutz, I. Gotlibovych, R. P. Smith, and Z. Hadzibabic, Phys. Rev. Lett. **110**, 200406 (2013).
[40] Q. Sun, L. Wen, W.-M. Liu, G. Juzeliūnas, and A.-C. Ji, Phys. Rev. A **91**, 033619 (2015).
[41] A. Aharony, J. Stat. Phys. **110**, 659 (2003).
[42] J. Langer, Ann. Phys. (N. Y.) **41**, 108 (1967).
[43] S. Coleman, Phys. Rev. D **15**, 2929 (1977); C. G. Callan, Jr., and S. Coleman, *ibid.* **16**, 1762 (1977).
[44] *Nucleation Theory and Applications*, edited by J. W. P. Schmelzer (John Wiley & Sons, Weinheim, 2006), p. 472.
[45] O. Fialko, B. Opanchuk, A. I. Sidorov, P. D. Drummond, and J. Brand, Europhys. Lett. **110**, 56001 (2015).
[46] C. Chen, R. Grimm, P. Julienne, and E. Tiesinga, Rev. Mod. Phys. **82**, 1225 (2010).
[47] It is well accepted that, in 1D or 2D SOC BECs, the superposition of opposite-momentum states yields an optimal mean-field ground-state wave function. We generalize this ansatz to 3D SOC BECs. See also Ref. [21].
[48] A. H. Guth and P. J. Steinhardt, Sci. Am. **250**, 116 (1984).
[49] R. Bousso, D. Harlow, and L. Senatore, Phys. Rev. D **91**, 083527 (2015).
[50] R. Mottl, F. Brennecke, K. Baumann, R. Landig, T. Donner, and T. Esslinger, Science **336**, 1570 (2012).
[51] L.-C. Ha, L. W. Clark, C. V. Parker, B. M. Anderson, and C. Chin, Phys. Rev. Lett. **114**, 055301 (2015).
[52] S.-C. Ji, L. Zhang, X.-T. Xu, Z. Wu, Y. Deng, S. Chen, and J.-W. Pan, Phys. Rev. Lett. **114**, 105301 (2015).
[53] M. A. Khamehchi, Y. Zhang, C. Hamner, T. Busch, and P. Engels, Phys. Rev. A **90**, 063624 (2014).
[54] Y. Li, G. I. Martone, L. P. Pitaevskii, and S. Stringari, Phys. Rev. Lett. **110**, 235302 (2013).
[55] A. Altland and B. Simons, *Condensed Matter Field Theory* (Cambridge University Press, Cambridge, 2006).
[56] C. Wu, M. Ian, and X. Zhou, Chin. Phys. Lett. **28**, 097102 (2011).